Three-Photon Absorption in Seeded CdSe/CdS Nanorod Heterostructures

ARTICLE *in* THE JOURNAL OF PHYSICAL CHEMISTRY C · AUGUST 2011

Impact Factor: 4.77 · DOI: 10.1021/jp205238q

5 AUTHORS, INCLUDING:

Sabyasachi Chakrabortty
Universität Ulm
16 PUBLICATIONS **207** CITATIONS
SEE PROFILE

Tze Chien Sum
Nanyang Technological University
144 PUBLICATIONS **3,513** CITATIONS
SEE PROFILE

THE JOURNAL OF PHYSICAL CHEMISTRY C

ARTICLE

pubs.acs.org/JPCC

Three-Photon Absorption in Seeded CdSe/CdS Nanorod Heterostructures

Guichuan Xing,[†] Sabyasachi Chakrabortty,[‡] Song Wee Ngiam,[†] Yinthai Chan,[‡] and Tze Chien Sum*[,†]

[†]Division of Physics and Applied Physics, School of Physical and Mathematical Sciences, Nanyang Technological University, Singapore 637371

[‡]Department of Chemistry, National University of Singapore, 3 Science Drive 3, Singapore 117543

Supporting Information

ABSTRACT: Size-dependent three-photon absorption (3PA) and three-photon-excited photoluminescence (PL) of CdSe/CdS nanorod heterostructures have been investigated using *Z*-scan and upconversion PL techniques with 150 fs laser pulses at 1300 nm. The PL from these rods shows clear cubic power dependence, and the 3PA cross section (σ_3) was found to be as high as 1.5×10^{-75} cm^6 s^2 photon^{-2} for 39 nm long rods, which is 2−4 orders of magnitude larger than those previously reported for spherical semiconductor nanocrystals under ∼100 fs laser pulse excitation. Importantly, by exploiting the unique property of the seeded nanorods to exhibit strong quantum confinement even at relatively large rod sizes, a superlinear dependence of the 3PA cross section on nanoparticle volume was found and validated over a wide volume range. A simple derived relation that quantitatively describes σ_3 and takes into account the laser pulse duration is proposed, thereby providing a clear basis of comparison between the σ_3 values of various II−VI semiconductor nanomaterials and facilitating a more judicious choice of their use in 3PA applications.

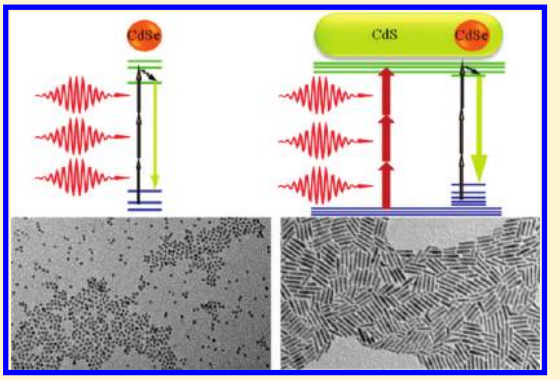

1. INTRODUCTION

Multiphoton absorption (MPA) is the simultaneous absorption of two or more photons that induces an electronic transition from the ground state to an excited state via virtual states. Energy conservation is fulfilled as the energy difference between these states matches the sum of the photons' energies.[1] In the last few decades, there have been extensive studies on the two-photon absorption (2PA) properties of semiconductor nanocrystals (NCs) with proposed applications in in vivo imaging, lasing, optical limiting, and three-dimensional data storage.[2−9] The complex relationships between the 2PA cross section and NC size,[3−5,8] shape,[5,6] and excitation wavelengths[6−8] have also been investigated, and several methodologies have been developed to enhance the 2PA cross section of semiconductor NCs to values as large as 10^{-44} cm^4 s/photon.[5,6] In contrast, research efforts on the three-photon absorption (3PA) of semiconductor NCs are still very limited despite its salient advantages over that of single- or two-photon excitation in bioimaging applications, which include (i) reduced volume of signal generation and (ii) higher spatial resolution and increased penetration depth when operating in the semitransparent window of biological media between 1100 and 1300 nm.[4,9−16]

One major impediment to the development of practical 3PA applications is the extremely small 3PA cross sections (σ_3) of these NCs that necessitate the use of high laser excitation fluences. Reported values for semiconductor NCs range from 10^{-77} to 10^{-79} cm^6 s^2 photon^{-2} under 100 fs laser pulse excitation.[4,9−13] Although it is clearly desirable to increase the σ_3 so that a lower laser fluence is needed and the risk of photodamage to samples can be reduced, simply increasing the volume of the NC in order to increase its absorption cross section can present a number of formidable difficulties. One obvious predicament is the fact that changing the volume and, therefore, size of these strongly quantum confined NCs inevitably shifts their emission wavelengths dramatically, which is highly undesirable for experiments with wavelength-specific requirements. Additionally, elucidating the volume dependence of the σ_3 over a wide range of NC volumes is, to the best of our knowledge, currently lacking, making it difficult to determine the optimal particle dimensions for various applications. This difficulty is further compounded by the dependence of the σ_3 values on the excitation laser pulse widths and the occurrence of 3PA-induced excited-state absorption (ESA) that augments the σ_3 values.

Herein, we show how these issues may be simultaneously addressed by employing seeded CdSe/CdS nanorod (NR) heterostructures, which comprise a spherical CdSe core located within a rodlike CdS shell. Beyond a certain rod length, these NR heterostructures exhibit nearly invariant photoluminescence (PL) peak emission and have volumes of about 1−2 orders of

Received: June 3, 2011
Revised: July 20, 2011
Published: August 03, 2011

magnitude larger than those in previously reported 3PA measurements,[4,9−13] resulting in very large σ_3 ($\sim 10^{-75}$ cm^6 s^2 photon^{-2}) that were determined using femtosecond *Z*-scan and validated using upconversion PL techniques at 1300 nm. This facilitated probing of the σ_3 over a much larger volume range than previously accessible. The dependence of σ_3 measurements on the excitation laser pulse duration was also investigated and compared with those of other efforts found in the existing literature. We subsequently derived a relation for σ_3 that provides a clear basis of comparison for the different σ_3 measurements of various II−VI semiconductor nanomaterials, so as to facilitate a more judicious choice of their use in applications utilizing 3PA excitation.

2. EXPERIMENTAL SECTION

2.1. Sample Preparation. The seeded CdSe/CdS NR heterostructures of three different lengths (i.e., 24, 34, and 39 nm) were prepared according to a previously published procedure[17] with slight modifications. Briefly, spherical CdSe cores of ~2.4 nm in size were first synthesized via the hot injection method as described in ref 18, followed by seeded growth of the CdS rodlike shell of different lengths at ~360 °C.[17]

2.2. Electron Microscopy and Steady-State Spectroscopy. The morphology and size distribution of the NRs were examined using a transmission electron microscope (JEOL-JEM 2010F) operating at 200 kV. Linear absorption measurements were carried out using a UV−vis-NIR spectrophotometer (Shimadzu, UV-3600). The one-photon (400 nm) excitation PL was collected with a Jasco FP-6300 spectrofluorometer.

2.3. 3PA and Time-Resolved PL. The room-temperature 3PA of CdSe/CdS NRs in toluene solution was investigated via the standard *Z*-scan technique.[19] Incident 1300 nm, 150 fs laser pulses were generated from a Coherent TOPAS-C optical parametric amplifier that was pumped using a 1 kHz Coherent Legend regenerative amplifier, which was seeded by a 80 MHz Coherent Vitesse oscillator. The low repetition rate of these laser pulses minimizes the possibility of any thermal effects. These input laser pulses were focused onto the samples using a lens with a focal length of 25 cm. The beam waist at the focal point was 30 ± 3 um. The samples were contained in 2 mm thick quartz cells, which were translated across the focal point using a linear translation stage along the beam propagation axis. The transmittance at different *z* positions was recorded. Room-temperature upconversion PL of these CdSe/CdS NRs was also investigated with the same excitation laser source as that used in the *Z*-scan. The laser pulses were focused by a lens (f = 25 cm) on the solution sample in a 2 mm thick quartz cell. The emission from the samples was collected at a backscattering angle of 150° by a pair of lenses and into an optical fiber that was coupled to a spectrometer (Acton, Spectra Pro 2500i) to be detected by a charge coupled device (Princeton Instruments, Pixis 400B). Time-resolved PL was collected using an Optronis Optoscope streak camera system that has an ultimate temporal resolution of 6 ps.

3. RESULTS AND DISCUSSION

The morphology and size distribution of the NRs were examined using a transmission electron microscope (TEM). Representative TEM images of these NRs are shown in Figure 1, where the rod diameters were measured to be ~5 nm (for all three samples), while the lengths were determined to be about 24, 34, and 39 nm, respectively. The length dispersions were less

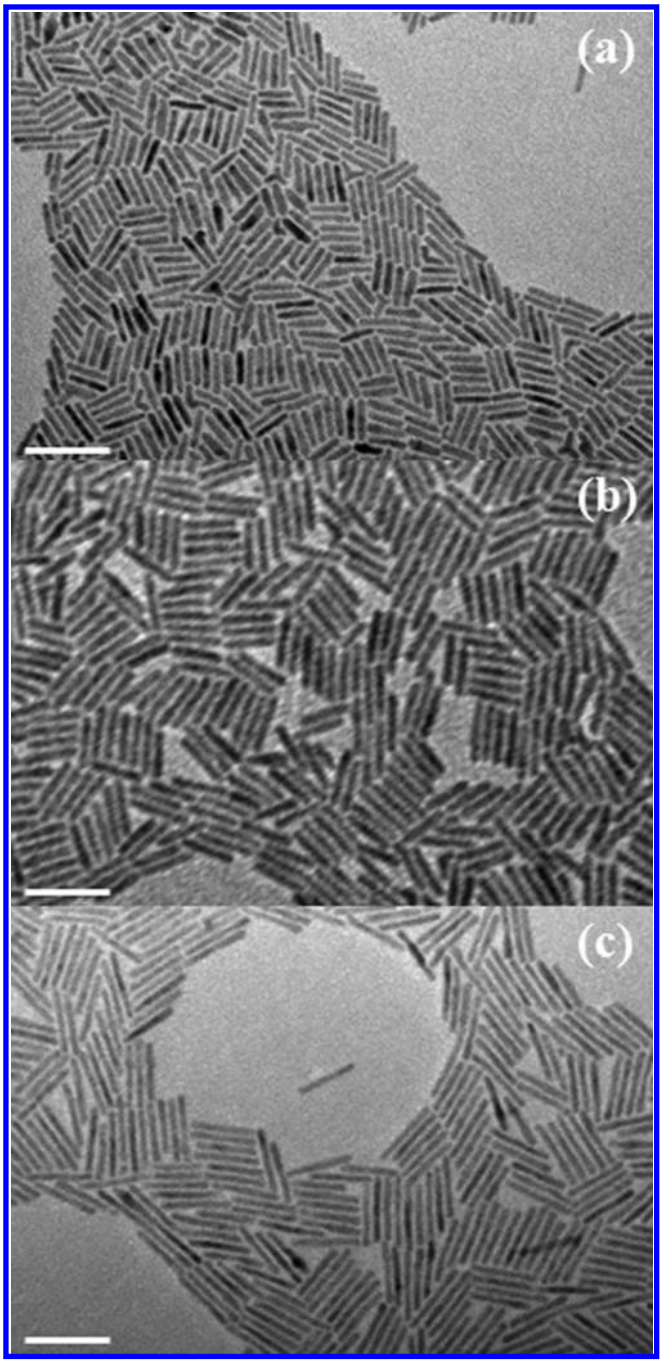

Figure 1. Panels a−c show the TEM images for 24, 34, and 39 nm long CdSe/CdS rods, respectively (white scale bar = 50 nm).

than 20% from over a hundred NRs measured. The normalized linear absorption results are shown in Figure 2a,c for dilute concentrations of NR samples in toluene. It is readily seen that there is a dominating absorption edge at around 480 nm, commensurate with the energy band gap of nanosized CdS.[5,6,17] The small absorption peak at lower energy (~580 nm) is attributed to the effective band edge transition in the CdSe core. Compared with the first absorption peak (at 509 nm) of the as-synthesized CdSe core in toluene, this value is significantly red shifted due to leakage of the electron wave function into the CdS shell. The PL originates from the recombination of the partially delocalized electron with the strongly localized hole in the CdSe core,[17] and Figure 2 shows

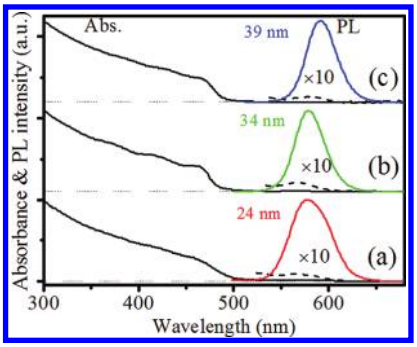

Figure 2. Panels a−c show the normalized UV−visible absorption spectra (black solid line) and its magnified (×10) region (black dashed line) and the 400 nm-excited PL spectra for 24 nm (red solid line), 34 nm (green solid line), and 39 nm (blue solid line) long CdSe/CdS rods respectively.

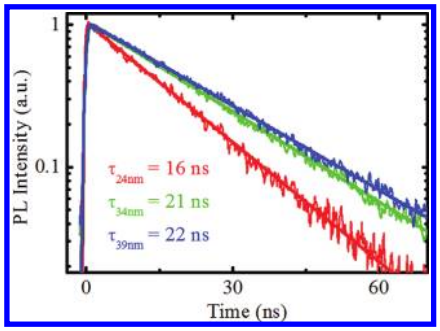

Figure 3. 400 nm-excited PL decay curves and the single-exponential fittings for 24, 34, and 39 nm CdSe/CdS rods.

the one-photon (400 nm) excitation PL spectra of seeded CdSe/CdS NRs of various lengths with an average Stokes shift of ∼10 nm. It should be noted that the PL peaks do not differ appreciably between the different rod lengths employed due to the exponential decay rate of the CdSe electron wave function leakage into the CdS shell; thus, no significant red shifts are expected beyond a certain rod length. Further tuning of the emission wavelength is achieved by varying the size of the CdSe core, which remains relatively strongly quantum-confined.

This trend of electron wave function leakage into the CdS shell is also evident from the transient PL lifetimes, further corroborating the wavelength invariance of the longer rods. The transient PL at the peak (±5 nm) of the CdSe/CdS NRs is given in Figure 3. These decay curves for all the samples are well fitted with a single-exponential decay function. The fitted lifetimes are 16, 21, and 22 ns for the 24, 34, and 39 nm rods, respectively. It can be seen that the PL lifetime increases with the NR length. Following photoexcitation, the photogenerated hole is localized to the size tunable core while the electron is delocalized partially into the shell. The electron−hole wave function overlap decreases with increasing rod length, and this is evident in the longer PL recombination lifetimes. The "plateauing" of the fluorescence lifetimes for these heterostructures suggests that, beyond a certain rod shell length, no further delocalization of the electron takes place, resulting in a further decline of the oscillator strength.

The room-temperature 3PA of CdSe/CdS NRs in toluene solution was investigated via the standard *Z*-scan technique[19] at 1300 nm. Figure 4a illustrates the typical open aperture *Z*-scan

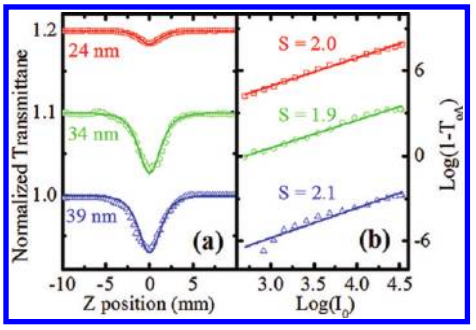

Figure 4. (a) Typical open aperture *Z*-scans at 1300 nm for 24 (red), 34 (green), and 39 nm (blue) CdSe/CdS nanodot/nanorod heterostructures. The solid lines are the fitting curves with eq 1. (b) The plots of $\log(1 - T_{OA})$ versus $\log(I_0)$; the solid lines represent the linear fits to the data.

responses of CdSe/CdS NRs of three different lengths at a pump intensity of 92 GW/cm^2 (I_{00}). The reduced transmittance at the focal point indicates the presence of nonlinear absorption in the NRs. Figure 4b depicts the log−log plots of absorbance ($1 - T_{OA}$) (where T_{OA} is the open aperture transmittance) as a function of the maximum laser intensity along the *Z* axis (I_0). Fitted slope values of ∼2 are indicative of the dominance of 3PA.[11−13] Following the open aperture *Z*-scan theory for 3PA, the normalized transmittance can be described as[1,19]

$$T_{OA}(z) = \frac{1}{\pi^{1/2} p_0} \int_{-\infty}^{\infty} \ln\{[1 + p_0^2 \exp(-2x^2)]^{1/2} + p_0 \exp(-x^2)\}\, dx \quad (1)$$

where $p_0 = (2\alpha_3 I_0^2 L'_{eff})^{1/2}$, $L'_{eff} = [1 - \exp(-2\alpha_0 L)]/(2\alpha_0)$, and α_0 and α_3 are the linear and 3PA absorption coefficients, respectively. L is the sample path length, $I_0 = I_{00}/(1 + z^2/z_0^2)$ is the incident intensity of the laser beam at z, I_{00} is the on axis peak power, and $z_0 = \pi\omega_0^2/\lambda$. From the fits, the 3PA coefficients per NR ($\alpha_{3\text{-NR}}$) obtained were 2.5, 5.5, and 6.3 ($\times 10^{-20}$ cm^3/GW^2), for the 24, 34, and 39 nm CdSe/CdS NRs, respectively. The σ_3 were then derived as 0.59, 1.3, and 1.5 ($\times 10^{-75}$) cm^6 s^2 photon^{-2} using the expression $\sigma_3 = \alpha_{3\text{-NR}}(\hbar\omega)^2$, where $\hbar\omega$ is the pump photon energy. The results obtained in this work, along with the reported 3PA cross sections for various II−VI semiconductor NCs, are summarized in Table 1.

Table 1 clearly shows that earlier 3PA studies in semiconductor NCs were mainly focused on colloidal semiconductor quantum dots (QDs) whose sizes are smaller than their exciton Bohr radius, resulting in the size-dependent tunability of their optoelectronic properties.[9−16] In the case of seeded CdSe/CdS NRs, photoabsorption occurs primarily in the large CdS shell that leads to an ultrafast hole localization to the CdSe core within 1 ps.[20] Hence, the CdS shell functions as a light-harvesting antenna whose shell dimension (length) can be tailored according to the requirements of a specific application, while the emission wavelength can be tuned by varying the size of the CdSe core. As shown in Table 1, our data clearly shows that the σ_3 increases with CdS shell length in CdSe/CdS NRs.

We compared the dependence of the σ_3 of the nanoparticles listed in Table 1 on their volume. It is obvious that the σ_3 should exhibit some dependence on the dimensions of the nanostructures. Previously, He et al. reported a σ_3 power-law dependence of 3.3 to the diameter of CdSe QDs in the strong quantum

Table 1. Sample, Excitation Pulse Parameters, Nanostructure Dimensions (D, Diameter; L, Length), and the Measured 3PA Cross Sections σ_3

sample	excitation pulse	dimensions (nm)	σ_3 (cm^6 s^2 photon^{-2})
CdSe/CdS NR[a]	150 fs, 1300 nm	D 5 × L 24	5.9×10^{-76}
		D 5 × L 34	1.3×10^{-75}
		D 5 × L 39	1.5×10^{-75}
Rhodamine 6G[a]	150 fs, 1300 nm		6×10^{-81}
CdS QD[10]	100 fs, 900−1000 nm	NA	$\sim 10^{-79}$
ZnS QD[11,13]	120 fs, 620−780 nm	D 1.3 and D 2.5	$\sim 10^{-78}$
CdSe QD[4]	160 fs, 1300 nm	D 2.0−3.9	$\sim 10^{-78}$
ZnSe/ZnS QD[12]	200 fs, 1000 nm	D 4.4	$\sim 10^{-77}$
Zn(Cu)Se/ZnS QD[12]		D 4.1	
SC-CdS QD[15]	25 ps, 1064 nm	D 2.5	$\sim 10^{-73}$
ZnSe QD[14]	35 ps, 1064 nm	D 3.5 and D 4.5	$\sim 10^{-75}$
ZnSe/ZnS QD[14]			
ZnS QD[16]	10 ns, 532 nm	D 3	$\sim 10^{-72}$
Zn(Mn)S QD[16]			

[a] Experimental uncertainty: ± 40%.

confinement regime.[4] To elucidate the dependence between nanostructures with differing geometries, we plotted our σ_3 data and those found in the existing literature (that was obtained with excitation pulses of ~100 fs) as a function of the NC volume in a log−log plot in Figure 5a.[4,11,12] From the fit, an empirical slope value of 1.5 ± 0.2 is obtained, suggesting a superlinear dependence between the σ_3 and the NC volume (regardless of the II−VI NC species). Importantly, this dependence was validated with nanoparticles of different material compositions and volumes ranging over 3 orders of magnitude, thus providing a firm basis for predicting the evolution of σ_3 with volume for a wide class of II−VI semiconductor nanoparticles. Under similar 100 fs laser pulse excitation, the σ_3 of our seeded CdSe/CdS NRs is 2−4 orders of magnitude larger than those previously reported for spherical semiconductor QDs.

To elucidate the dependence between the measured σ_3 values and the pulse duration of the excitation pulses between different nanomaterials with differing geometries, we plotted the volume-normalized σ_3 against the excitation pulse duration in a log−log plot in Figure 5b and compared them against the theoretical values calculated using a simple 3PA/3PA-induced excited-state absorption (ESA) model shown in Figure 5b, inset. The data used are from this work as well as those found in the literature for the various II−VI NC species, with the laser excitation pulse widths spanning 5 orders of magnitude.[4,11−16] Typically, larger σ_3 values are obtained for measurements performed with longer (i.e., picosecond or nanosecond) excitation pulses. These measured σ_3 values are usually an overestimate of the intrinsic σ_3 values by several orders of magnitude due to increased contributions from ESA and increased scattering from microbubble formation caused by thermal effects.[1,21]

In our model, under the thin sample approximation, the change in the light intensity caused by 3PA and 3PA-induced ESA within the sample can be described as

$$\frac{\partial I}{\partial z'} = -\alpha_3 I^3 - \sigma_{ex} N_{eh} I \qquad (2)$$

where z' is the propagation length inside the samples, σ_{ex} is the ESA cross section, and N_{eh} is the 3PA generated electron−hole

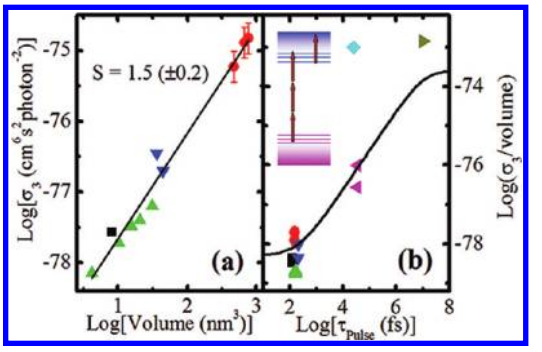

Figure 5. (a) The plot of log(σ_3) versus log(volume). The experiments were conducted with 100 fs laser pulses. The solid lines represent the linear fits to the data. (b) The plot of log(σ_3/volume) versus log(τ_{pulse} pulse duration). The solid line is the theoretical fit using eq 4 derived from our model. The experimental results were taken from ref 11 (black square), present work (red circle), ref 4 (green triangle up), ref 12 (blue triangle down), ref 15 (blue diamond), ref 14 (purple triangle left), and ref 16 (gold triangle right). The inset of (b) shows the schematic diagram of the 3PA and 3PA-induced ESA process.

pair density and is governed by

$$\frac{\partial N_{eh}}{\partial t} = \frac{\alpha_3 I^3}{3\hbar\omega} - \frac{N_{eh}}{\tau_{eh}} \qquad (3)$$

where τ_{eh} is the lifetime of the carriers in the excited state. We have also assumed that the ground state has an abundance of carriers and is not depleted following the pulsed excitation. The observed effective 3PA cross section ($\sigma_{3\text{-effective}}$) as a function of the intrinsic 3PA cross section (σ_3) can then be described as

$$\sigma_{3\text{-effective}} = \sigma_3 \left[1 + \frac{\int_{-\infty}^{\infty} \sigma_{ex} N_{eh} I(t)\, dt}{\int_{-\infty}^{\infty} \alpha_3 I(t)^3\, dt} \right] \qquad (4)$$

For laser pulses with a Gaussian temporal profile, $I(t) = I_0 \exp(-t^2/\tau_p^2)$, where τ_p is the pulse duration and I_0 is the incident

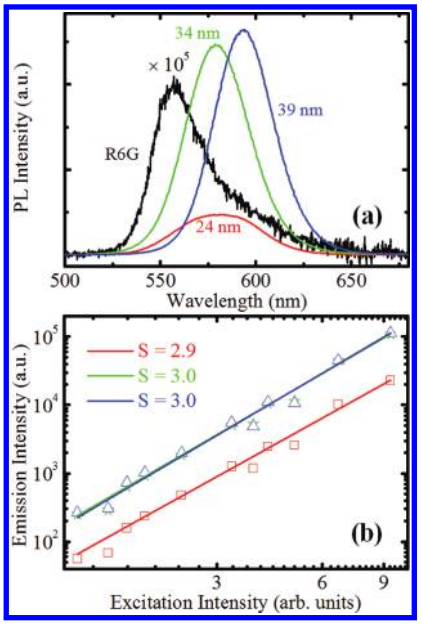

Figure 6. (a) Three-photon-excited PL spectra of 24 (red), 34 (green), and 39 nm (blue) CdSe/CdS rods in toluene are compared with that of Rhodamine 6G (black) in methanol. The PL spectra were obtained with a 1300 nm excitation wavelength at 60 GW/cm^2 and were normalized by the particle (molecule) number concentration. (b) Log−log plots for the PL signals as a function of the excitation intensity.

pulse intensity. On the basis of eq 4, $\sigma_{3\text{-effective}}$ is calculated to increase with increasing pulse intensity and pulse duration. For a fixed incident pulse intensity of I_0 = 50 GW/cm^2, and using typical parameters for a semiconductor NC (i.e., τ_{eh} = 10 ns, λ_{ex} = 1300 nm (i.e., $\hbar\omega$ = 0.95 eV), $\sigma_{ex} = 5 \times 10^{-17}$ cm^2, and $\sigma_3 = 5 \times 10^{-79}$ cm^6 s^2 photon^{-2}), the calculated $\sigma_{3\text{-effective}}$ (solid line) against the excitation pulse duration is plotted in a log−log scale in Figure 5b. Our choice of these values is further justified in the Supporting Information, where it is shown that, within the extrema of the reported values for I_0, τ_{eh}, and λ_{ex}, these parameters have a relatively insignificant effect over the dependence of the volume-normalized $\sigma_{3\text{-effective}}$ on τ_p. Most significantly, Figure 5b clearly shows that the theoretical prediction was validated with the reported experimental 3PA values for NCs of different material compositions and excitation laser pulse widths ranging over 5 orders of magnitude.

For 100 fs laser pulses, the observed nonlinear absorption is dominated by the intrinsic σ_3 (i.e., the first term of eq 4) that is dictated by the three-photon transition probability.[22] However, from eq 3, N_{eh} increases with increasing pulse duration (i.e., τ_p, which is embedded in $I(t)$); the contribution from the 3PA-induced ESA in eq 4 (i.e., the second term) thus increases for longer pulses. Nonetheless, contributions to ESA will eventually saturate (see Figure 4b) when the excitation pulse duration becomes comparable with τ_{eh} (from eq 3) as the excited carriers recombine, reducing N_{eh} and hence the contributions from the second term of eq 4. Although 3PA-induced ESA is useful for optical limiting applications, it is undesirable for applications in frequency upconversion imaging and lasing as it depletes the N_{eh} population at the excited state, through the excitation of these carriers at the excited state to the higher-energy states.

In retrospect, Figure 5a,b clearly shows that the σ_3 of semiconductor NCs measured by nonlinear absorption experiments is greatly dependent on the NC volume and the pulse duration of the excitation laser and exhibits less dependence on the material type and excitation wavelengths used. We have thus proposed simple relations that provide a firm basis for predicting the evolution of the 3PA cross section with volume as well as that with the excitation laser pulse duration for a wide class of II−VI semiconductor nanoparticles, which will be essential in guiding the development and the applications of such nanomaterials utilizing 3PA excitation.

In tandem with the investigations of the 3PA-induced PL properties of our CdSe/CdS NRs, a complementary approach from considering the upconversion PL intensity was also taken to further assess the validity of the σ_3 values (derived from the *Z*-scan measurements) for our NRs. Given that

$$F \sim \eta\sigma_3\varphi\rho I^3 \tag{5}$$

where F is the 3PA-induced PL intensity, η is the PL quantum yield, σ_3 is the 3PA cross section, φ is the fluorescence collection efficiency of the experimental setup, ρ is the sample concentration, and I is the pump laser intensity within the sample. The last three variables of eq 5 (i.e., φ, ρ, and I) can be kept constant in the experiment and η can be found through standard fluorescence quantum yield measurements. The ratios of the σ_3 for the various seeded nanorods could thus be found from the ratios of the 3PA-induced PL intensities and compared with the ratios found earlier from the *Z*-scan measurements. These values were also benchmarked against that of a standard dye (Rhodamine 6G (R6G)) commonly used for multiphoton applications.

Figure 6a shows the 1300 nm-excited upconversion PL spectra of the CdSe/CdS NRs and that of R6G. These spectra were collected under the same experimental conditions and normalized by the particle number (molecule) concentration. Figure 6b shows the power-dependent PL as a function of the excitation intensity. All samples possessed a cubic dependence, confirming that the PL was indeed induced by 3PA. Figure 6a clearly shows that the 3PA-induced PL intensity from the CdSe/CdS NRs is ∼5 orders larger than that of R6G. From the quantum yields (η), 32, 61, 56, and 95%, measured for the 24, 34, and 39 nm CdSe/CdS NRs and R6G, respectively, the ratio of the σ_3 between these samples was found to be (9.3×10^4):(2.0×10^5):(2.2×10^5):1. This σ_3 ratio among the CdSe/CdS NRs is closely matched with the results obtained from the *Z*-scan, thus providing greater confidence for our reported σ_3 values for our NRs. Lastly, the σ_3 of R6G was also found to be 6 ($\pm$3) $\times 10^{-81}$ cm^6 s^2 photon^{-2}, a value that is about 6 orders of magnitude smaller than that of CdSe/CdS NRs.

4. CONCLUSIONS

Size-dependent 3PA and 3PA-induced PL properties of seeded CdSe/CdS NR heterostructures have been studied by *Z*-scan and upconversion PL measurements with 150 fs, 1300 nm laser pulses. The 3PA cross section is found to be as large as 1.5 $\times$ 10^{-75}cm^6 s^2 photon^{-2} for the 39 nm rods, which is 2−4 orders of magnitude larger than that of the previously reported spherical semiconductor QDs and 6 orders of magnitude larger than that of R6G. With high quantum yields (>30%), the PL exhibits a clear cubic power dependence and the PL lifetimes increase with the rod length. That the greatly enhanced 3PA cross sections are attainable strongly suggests that such seeded CdSe/CdS NRs hold great promise for nonlinear optical applications. Under 100 fs laser pulse excitation, the σ_3 of the II−VI semiconductor nanomaterials is found to exhibit a superlinear dependence on the NC volume and is independent of the II−VI

NC species. The experimentally reported σ_3 values of semiconductor NCs are strongly dependent on the excitation laser pulse duration and could be well-modeled using a 3PA/3PA-induced excited-state absorption (ESA) model. Typically, excitation with longer laser pulses results in an overestimation of the 3PA cross section due to additional contributions from increased excited-state absorption (ESA) and increased scattering from microbubble formation. From the validation of these dependences in II−VI semiconductor nanocrystals of different compositions over NC volumes spanning 3 orders of magnitude and excitation laser pulse widths spanning 5 orders of magnitude, we have thus proposed simple dependences/relations to provide a clear and unambiguous basis of comparison of their nonlinear properties that will facilitate the design and selection of such nanomaterials for 3PA applications.

■ ASSOCIATED CONTENT

Supporting Information. These include the spectral characterization data of the CdSe core and the details on the 3PA/3PA-induced excited-state absorption model. This material is available free of charge via the Internet at http://pubs.acs.org.

■ AUTHOR INFORMATION

Corresponding Author
*E-mail: tzechien@ntu.edu.sg.

■ ACKNOWLEDGMENT

This work is supported by a NTU start-up grant (M58110068); an Academic Research Fund (AcRF) Tier 1 grant, RG 49/08 (M52110082); the SPMS Research Collaborative Award (M58110090); and a NUS start-up grant (WBS-R143-000-367-133).

■ REFERENCES

(1) Sutherland, R. L. with contributions by Mclean, D. G.; Kirkpatrick, S. *Handbook of Nonlinear Optics*, 2nd ed.; Marcel Dekker: New York, 2003.
(2) Larson, D. R.; Zipfel, W. R.; Williams, R. M.; Clark, S. W.; Bruchez, M. P.; Wise, F. W.; Webb, W. W. *Science* **2003**, *300*, 1434–1436.
(3) Pu, S. C.; Yang, M. J.; Hsu, C. C.; Lai, C. W.; Hsieh, C. C.; Lin, S. H.; Cheng, Y. M.; Chou, P. T. *Small* **2006**, *2*, 1308–1313.
(4) He, G. S.; Yong, K. T.; Zheng, Q. D.; Sahoo, Y.; Baev, A.; Ryasnyanskiy, A. I.; Prasad, P. N. *Opt. Express* **2007**, *15*, 12818–12833.
(5) Xing, G. C.; Chakrabortty, S.; Chou, K. L.; Mishra, N.; Huan, C. H. A.; Chan, Y.; Sum, T. C. *Appl. Phys. Lett.* **2010**, *97*, 061112.
(6) Li, X. P.; Embden, J.; van; Chon, J. W. M.; Gu, M. *Appl. Phys. Lett.* **2009**, *94*, 103117.
(7) Fedorov, A. V.; Baranov, A. V.; Inoue, K. *Phys. Rev. B* **1996**, *54*, 8627–8632.
(8) Padilha, L. A.; Nootz, G.; Olszak, P. D.; Webster, S.; Hagan, D. J.; Van Stryland, E. W.; Levina, L.; Sukhovatkin, V.; Brzozowski, L.; Sargent, E. H. *Nano Lett.* **2011**, *11*, 1227–1231.
(9) Xing, G. C.; Ji, W.; Zheng, Y. G.; Ying, J. Y. *Appl. Phys. Lett.* **2008**, *93*, 241114.
(10) Chon, J. W. M.; Gu, M.; Bullen, C.; Mulvaney, P. *Appl. Phys. Lett.* **2004**, *84*, 4472.
(11) He, J.; Ji, W.; Mi, J.; Zheng, Y. G.; Ying, J. Y. *Appl. Phys. Lett.* **2006**, *88*, 181114.
(12) Xing, G. C.; Ji, W.; Zheng, Y. G.; Ying, J. Y. *Opt. Express* **2008**, *16*, 5710–5715.
(13) He, J.; Scholes, G. D.; Ang, Y. L.; Ji, W.; Beh, C. W. J.; Chin, W. S. *Appl. Phys. Lett.* **2008**, *92*, 131114.
(14) Lad, A. D.; Kiran, P. P.; Kumar, G. R.; Mahamuni, S. *Appl. Phys. Lett.* **2007**, *90*, 133113.
(15) Gao, Y.; Tonizzo, A.; Walser, A.; Potasek, M.; Dorsinville, R. *Appl. Phys. Lett.* **2008**, *92*, 033106.
(16) Chattopadhyay, M.; Kumbhakar, P.; Sarkar, R.; Mitra, A. K. *Appl. Phys. Lett.* **2009**, *95*, 163115.
(17) Carbone, L.; Nobile, C.; De Giorgi, M.; Della Sala, F.; Morello, G.; Pompa, P.; Hytch, M.; Snoeck, E.; Fiore, A.; Franchini, I. R.; Nadasan, M.; Silvestre, A. F.; Chiodo, L.; Kudera, S.; Cingolani, R.; Krahne, R.; Manna, L. *Nano Lett.* **2007**, *7*, 2942–2950.
(18) Snee, P. T.; Chan, Y.; Nocera, D. G.; Bawendi, M. G. *Adv. Mater.* **2005**, *17*, 1131–1136.
(19) Sheik-Bahae, M.; Said, A. A.; Wei, T. H.; Hagan, D. J.; Styland, E. W. V. *IEEE J. Quantum Electron.* **1990**, *26*, 760–769.
(20) Lupo, M. G.; Sala, F. D.; Carbone, L.; Zavelani-Rossi, M.; Fiore, A.; Luer, L.; Polli, D.; Cingolani, R.; Manna, L.; Lanzani, G. *Nano Lett.* **2008**, *8*, 4582–4587.
(21) Tutt, L. W.; Boggess, T. F. *Prog. Quantum Electron.* **1993**, *17*, 299–338.
(22) Yee, J. H. *Phys. Rev. B* **1972**, *5*, 449–458.